THESIS FOR THE DEGREE OF LICENTIATE OF ENGINEERING

3D modelling of epidermal nerve fiber patterns

Konstantinos Konstantinou

CHALMERS
UNIVERSITY OF TECHNOLOGY

Division of Applied Mathematics and Statistics
Department of Mathematical Sciences
Chalmers University of Technology
Göteborg, Sweden 2022

3D modelling of epidermal nerve fiber patterns
Konstantinos Konstantinou
Göteborg 2022

Division of Applied Mathematics and Statistics
Department of Mathematical Sciences
Chalmers University of Technology
SE-412 96 Göteborg
Sweden
Telephone +46 (0)31 772 1000

Typeset with LaTeX
Printed in Göteborg, Sweden 2022

3D modelling of epidermal nerve fiber patterns

Konstantinos Konstantinou

Division of Applied Mathematics and Statistics
Department of Mathematical Sciences
Chalmers University of Technology

Abstract

Neuropathical disorders, such as diabetic neuropathy, damage the nerve structure in the epidermis. This thesis presents statistical analyses and models for the epidermal nerve fibers (ENFs). The main objective is to improve our understanding regarding the three dimensional ENF structure and for this purpose, stochastic models are constructed. The ENF data are treated as point process configurations in three dimensional boxes, and samples from mild diabetic subjects and healthy volunteers are considered. In Paper I, the structure of the nerve trees is analyzed by comparing distributional properties of the first and later nerve tree segments. Using tools from spatial point process theory, second order properties of the underlying processes are examined and compared. We also defined a new measure, called epidermal active territory, to measure the volume of the epidermis covered by the nerves. Further, a three dimensional point process model for the nerve structure, is developed and evaluated using spatial summary statistics. The two dimensional version of the model captured the planar spatial structure, however, the complete model was unable to capture the attraction between the nerve fiber endings in the data. Therefore, a pairwise interaction Markov model allowing neighboring end points to interact was proposed in Paper II. Due to the anisotropic nature of the data, directional summary statistics were used to assess the goodness of fit of the models. The model was able to capture the attraction between the nerve fiber endings in the data.

Keywords: Anisotropy, diabetic neuropathy, epidermal nerve fibers, point processes.

List of publications

This thesis is based on the work represented by the following papers:

I. **Konstantinou, K.** and Särkkä, A.(2021). Spatial modeling of epidermal nerve fiber patterns *Statistics in medicine*, doi: https://doi.org/10.1002/sim.9194.
II. **Konstantinou, K.** and Särkkä, A.(2021). Pairwise interaction Markov model for the 3D epidermal nerve fiber endings. Submitted in *Statistic in Medicine*.

Author contributions

I. I developed the two-step NOC-like model and extended the concept of reactive territories in three dimensions. I implemented the methods and conducted all statistical analyses. I did most of the writing of the publication.

II. I implemented the estimation methods of the pairwise interaction Markov field model and carried out the simulation study. I conducted all statistical analyses and did most of the writing of the publication.

List of Figures

Acknowledgements

First and foremost, I want to express my sincere gratitude to my supervisor Aila Särkkä for introducing me to the wonderful subject of spatial point processes, for always being available to meet and advise me and for always carefully reading and providing constructive feedback on my manuscripts. Thank you Aila for your continuous support and encouragement. I also want to thank my co-supervisors, Umberto Picchini and Ottmar Cronie, as well as my examiner Petter Mostad, for the fruitful discussions and guidance. I'd like to thank William R. Kennedy, Gwen Wendelschafer-Crabb, and the other members of the Kennedy Lab for sharing the epidermal nerve fiber data, as well as Adam Loavenbruck for addressing my neurology and data-related questions.

I want to express my sincere gratitude to the Swedish Research Council for financially supporting my research, as well as the Chalmersska forskningsfonden grant for covering my conference related expenses. This work would not have been possible without their contribution. I am also grateful to all my colleagues in the mathematical department for making this such a lovely workplace. I would also like to thank all the department's administrative staff for always being willing and able to help me with any non-mathematical issues that come up.

Finally, I would like to express my gratitude to my friends and family for their love, continuous encouragement, and unwavering support. This thesis would not have been feasible without them.

Contents

1 Introduction

Epidermal nerve fibers (ENF) are dendroidal, unmyelinated thin sensory nerve fibers found in the epidermis, the skin's outermost living layer. They pass across dermis, the skin layer beneath the epidermis, enter and grow within the epidermis with or without branching until they terminate (see Figure 2.1). The ENF endings are responsible for transferring signals such as pain and heat to the central nervous system. Peripheral neuropathies, such as diabetic neuropathy, a neuropathic disorder caused by diabetes, damage the nerves. This damage translates into symptoms such as neuropathic pain and loss of sensation. As there is no current treatment able to restore the nerve fibers functionality, diagnosis of the neuropathy at an early stage is important.

After some improved imaging procedures for visualisation and detection of ENFs had been established in the early nineties, research focus shifted towards the potential diagnostic capabilities of ENFs (Kennedy and Wendelschafer-Crabb, 1993; Kennedy et al., 1996, 1999). Epidermal nerve fiber data can be collected through suction induced skin biopsies, a procedure where a portion of the epidermis is removed, mounted on a slide and stained for imaging. Confocal microscopy is then used to manually trace the locations where the nerve fibers enter the epidermis, branch and terminate (Kennedy and Wendelschafer-Crabb, 1993). Throughout this thesis, those points will be referred to as base, branch and end points, respectively. Spatial point pattern data from healthy volunteers and diabetic patients obtained from different body parts are available. For our statistical analyses, we treat the base, branch and end points as realisations of point processes in three dimensional boxes. The observational boxes have fixed lengths and widths, and varying heights that depend on the local thickness of the epidermis.

The earliest research findings suggest that there is a negative correlation between the spatial intensity of the base and end point patterns with the degree of the neuropathy (Kennedy et al., 1996, 1999). Based on this observation some diagnostic tools have been developed. In particular, the current clinical practice

is based on the normative reference ranges of the intraepidermal nerve fiber density that was established in a series of studies (Lauria et al., 2010). Moreover, the negative correlation between the degree of the neuropathy and total ENF coverage of the epidermis is discussed in many studies (Waller et al., 2011; Myllymäki et al., 2012; Andersson et al., 2016; Olsbo et al., 2013). The reduction of the total ENF coverage is strongly related with the observed symptoms, i.e loss of sensation and neuropathic pain. However, those physiological changes do not occur simultaneously throughout the body. The skin samples obtained from more distant body parts like feet poses higher diagnostic value than the skin samples from e.g thigh and calf. Therefore, in our analyses we considered only ENF data obtained from feet (Kennedy et al., 1999).

Several studies propose clustered point process models for the planar spatial structure of the ENFs end points (Olsbo et al., 2013; Andersson et al., 2016; Ghorbanpour et al., 2021; Garcia et al., 2020). Here, we are particularly interested in the so-called Non-Orphan Cluster (NOC) model developed by Olsbo et al. (2013) and the Uniform Cluster Centre (UCC) model developed by Andersson et al. (2016). In the NOC and UCC models the end point clusters are constructed conditioned on the empirical base point patterns. The main difference of the models is the end point cluster direction, i.e the direction of the end point clusters with respect to their corresponding base points. In the UCC model there is no preferred direction, while in the NOC model the end point clusters are constructed toward open space. The direction opposite to the closest other base point was used to approximate the open space direction. Point process model for the base point patterns are suggested in Andersson et al. (2019) and Andersson and Mrkvička (2020). Even the base points were found to be clustered indicating that the nerve fibers may branch prior to entering the epidermis.

The main goal of this thesis is to further enhance our understanding of the biological process that leads the morphological alterations in nerve fibers caused by neuropathy. Better understanding of the underlying process can contribute to the development of more efficient techniques for early identification of the disease. To achieve our objectives, we investigated the three-dimensional structure of the nerve trees. Unlike the previous models that solely examine the base and end point locations, we included the first branching points in the analyses.

In Paper I, the three dimensional structure of the ENFs endings was investigated, to the best of our knowledge, for the first time. The nerve tree structure within the individual nerve fibers and between the disease groups was investigated. Our findings indicate that the segments connecting the end and branching points in the two groups have significant distributional differences. Then, we examined possible competitive behaviours between the nerve fibers.

For this purpose, the concept of epidermal active territory (EAT), a tool that approximates the volume of the epidermis covered by the nerve trees was introduced. The EAT values for each individual nerve tree were then attached as marks to the base point patterns. No evidence was found to suggest that the nerve fibers compete with each other in terms of mark correlation. Finally, we constructed a three-dimensional two-step spatial point process model for the end points that includes some ingredients from the NOC and UCC models. In the first step, the branching point locations are constructed towards open space, as in the NOC model, while in the second step, the end point clusters are constructed around the branching points, as in the UCC model. The two-dimensional version of the model fitted the data quite well while the 3D version failed to capture the structure of the data at intermediate distances.

The model proposed in Paper I was further developed in Paper II. This extension allowed interaction between nerve fiber end points. In this model, the planar point patterns were simulated using the 2D version of the initial model. Then, the z-coordinates of the points were constructed using a pairwise interaction Markov field model (Christoffersen et al., 2021). For evaluating the model we considered samples from two healthy and two mild diabetic subjects. To assess the goodness of fit we used directional summary functions from spatial statistics due to the anisotropic nature of the data. We found some indication of variations in the degree of interaction and the extent of the interaction zone between the groups.

The thesis is structured as follows. In Section 2, we describe the epidermal nerve fiber dataset and in Section 3, we briefly present some theoretical aspects of the point process theory and in Section 4, present some additional statistical tools. A brief summary of the appended papers is given in Section 5. Discussion about the main contributions and future work are presented in Section 6.

2 Data

The epidermal nerve fiber dataset is a hierarchically structured point pattern collection comprising data from healthy volunteers and diabetic patients. The main hierarchies are the degree of diabetic neuropathy, i.e healthy, mild, moderate or severe, the different subjects and samples within the subjects. As the primary goal of this thesis is to investigate neuropathy at the earliest feasible stage, we concentrated on data collected from 8 mild diabetic subjects and 32 healthy controls. Furthermore, data from each subject's feet, calves, and thighs are available. However, we focus on the foot data since research has shown that changes in the physiology of the ENFs occur at an early stage in the distant body regions (Andersson et al., 2016). For each subject, three to six skin samples are available. The ENF dataset further contains non-spatial covariates such as age, BMI and gender which are not considered in the spatial analyses in this thesis.

The data are modeled as point processes in a three-dimensional box. Each point pattern contains three different types of points: base, branch, and end points. Despite the fact that the base points are the locations, where the nerves enter the epidermis, their height values fluctuate because the base of the epidermis is not totally flat. Since the nerve fibers may branch in deeper skin layers the base points are clustered. The second type of points that are of interest are the first branching points, which will be referred to as branching point throughout the thesis. Those are the points where the fibers begin to branch in the epidermis. The epidermal nerve fiber endings are the third type of points. Those are the points responsible for feeling heat and pain and hence their spatial structure is important. Similarly to the base points, the end point configurations are also clustered.

In the statistical analyses conducted in this thesis, an epidermal nerve tree is represented by its base, first branching and end points. The structure of the ENF data is presented in Figure 2.1. The segments connecting the branching points and other types of points are also presented to offer a more accurate

representation of the nerve tree structure.

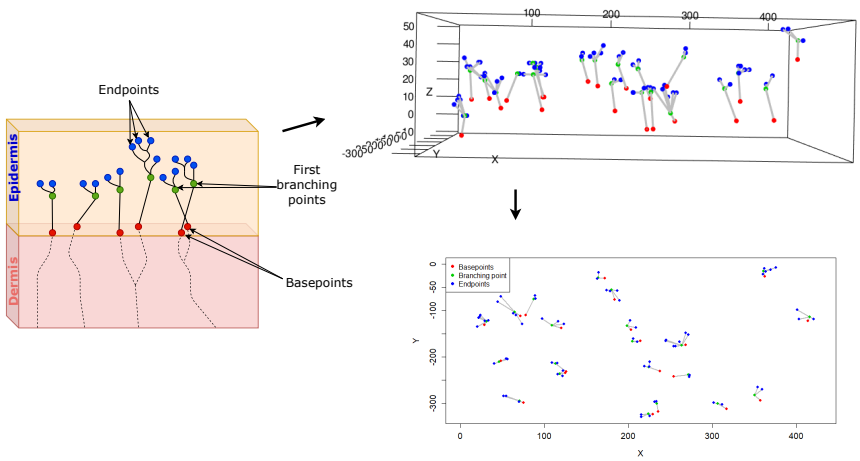

Figure 2.1: An illustration of the ENF data structure (left). An example of the three dimensional multi-type point patterns of the ENF base, branch and end points (top right). The corresponding two dimensional point pattern of the projections of the ENF base, branch and end points (bottom right). The connections between the branching points and the base and end points are also illustrated.

3 Spatial point processes

The aim of this chapter is to provide a brief introduction to the theoretical concepts used throughout the thesis. In the chapter, basic concept definitions and a brief overview of spatial summary functions for spatial point processes are recalled and discussed. For a more mathematically rigorous treatment to the subject, the reader is referred to the literature (Illian et al., 2008; Møller and Waagepetersen, 2004; Chiu et al., 2013). The definitions and notations given here mainly follow the book by Illian et al. (2008). Throughout this work $\mathbb{R}^d$ and $\mathcal{B}(\mathbb{R}^d)$, denote the d-dimensional Euclidean space and its corresponding Borel sets, respectively. The indicator function is denoted by $\mathbb{I}\{\cdot\}$ and the $\neq$ above summation sign denotes the summation over all distinct pairs.

3.1 Basic definitions

Spatial point processes are mathematical models suitable for characterising a random set of points. A point process describes the stochastic probabilistic rule that constructs point patterns according to a certain distribution. The process is usually defined in the entire spatial domain $\mathcal{D}$, but is only observed in an observational window $W \subset \mathcal{D}$. Realisations of point processes are called point patterns or point configurations and the points are often referred to as events. Point processes are central in many applications and serve as models for a wide range of physical phenomena. Such applications include astronomy, which involves modeling the spatial locations of galaxies and stars, forestry, which involves modeling the spatial distribution and interactions between e.g. different tree species, and medical applications, for instance modeling the changes in the spatial structure of the termination locations of epidermal nerve fibers as diabetic neuropathy progresses. The latter application is the subject of this thesis.

The point processes are assumed to be *simple*, meaning that at every distinct location the process place at most one point, and *locally finite*, indicating that for every bounded Borel set B, the random variable $N_X(B)$ associated with the number of the points of the process $X = \{X_i\}$ in B, is finite. The notation X_i, denotes the locations of random points in D. In mathematical notation this is written as follows.

(i) X is simple $\iff \mathbb{P}(X_i \neq X_j) = 1, \quad \forall\, i \neq j$

(ii) X is locally finite $\iff \forall B \in \mathcal{B}(\mathbb{R}^d)$ that is bounded, we have that $N_X(B) < \infty$

The *intensity measure* of a point process, $\Lambda(B) : \mathcal{B}(\mathbb{R}^d) \to [0, \infty)$, is defined as the expected number of points of the process X in B, i.e $\Lambda(B) \equiv E[N_X(B)]$. In applications, the intensity measure $\Lambda(B)$ can be assumed to be absolutely continuous with respect to the Lebesgue measure, hence it can be expressed as

$$\Lambda(B) = \int_B \lambda(x)dx, \tag{3.1}$$

where the function $\lambda : \mathcal{B}(\mathbb{R}^d) \to [0, \infty)$, is called the *intensity function*.

A point process X is *stationary* if its distribution is invariant under translations. For stationary point processes, and hence translation invariant measures, a measure theoretic result states that the intensity measure should be a multiple of the Lebesgue measure $|\cdot|$, i.e $\Lambda(B) = \lambda \mid B \mid$, which implies that the intensity function $\lambda(x) \equiv \lambda$. Since the intensity function is constant, it is often referred as the intensity or point density of the process, and may be interpreted as the mean number of points per unit area. On the other hand, proving the stationarity assumption of the underlying process from just one realisation is statistically impossible, and justifying stationarity is mainly based on application related arguments. Lastly, a point process X is *isotropic* if its distribution is invariant under rotations around the origin. In the appended Papers, the point patterns containing the projections of the ENF base, branch and end points into the plane, are assumed to be realizations from stationary and isotropic point processes. However, the three dimensional point patterns are assumed to be stationary but not isotropic.

There are three main types of point patterns, namely clustered, regular and completely spatially random (CSR) patterns. In a clustered pattern, there are attractive spatial dependencies between the points, in a regular pattern, there are repulsive dependencies between the points and in the CSR patterns, there is no structure, i.e the points are uniformly and independently distributed

in space. An illustration of the three main types of points patterns is given in Figure 3.1. More complicated types of point processes may be created by incorporating different type of dependencies at different scales, for instance a clustered pattern with repulsion between the clusters. Therefore, characterizing the structure of the point pattern data at hand is one of the key research topics in point process theory.

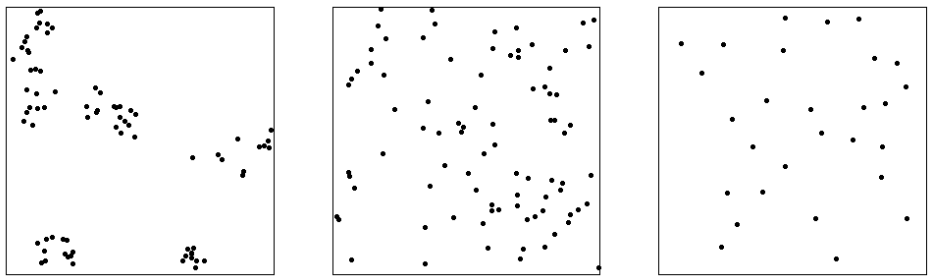

Figure 3.1: The three main types of point patterns: clustered (left), completely spatially random (middle) and regular (right).

3.1.1 Poisson point process

The Poisson point process is a mathematical model describing the complete spatial randomness case. A point process is a homogeneous Poisson point process with intensity $\lambda \geq 0$ if

(i) The random number of points of the process in a set B follows a Poisson distribution with the expectation $\lambda \mid B \mid$, i.e $N_X(B) \sim Pois(\lambda \mid B \mid)$, and

(ii) Conditioned on $N_X(B) = n$, the points are uniformly and independently allocated in B.

Despite its simplicity the Poisson process has a fundamental role in the characterisation of the spatial structure of spatial point patterns. As many theoretical properties and spatial summary functions can explicitly be derived for the Poisson point process, it is used as a reference model. That is, the summary functions estimated from empirical point patterns are compared to the theoretical values under CSR.

Furthermore, it serves as a basic building block for constructing more complex clustered and regular point processes. For instance, it serves as a model for

the parent process in Neyman-Scott point processes, a family of models for clustered point patterns (see Section 3.3.1), as well as a model for the parent process in hardcore type of processes, a family of models for regular point patterns.

3.2 Functional summary statistics

We recall that the ENF base, branch and end points are treated as realisations of stationary point processes in a three-dimensional box. In this section, functional summary statistics for stationary point processes are briefly recalled.

3.2.1 Distribution functions

The *empty space distribution function* $F(r) : [0, \infty) \to [0, 1]$ gives the probability that the ball around an arbitrary point $x \in \mathbb{R}^d$ with radius r, $b(x, r)$ contains at least one event of the point process X. For stationary point processes, it is sufficient to consider x to be the origin o. In mathematical notation, $F(r)$ is expressed as

$$F(r) = 1 - \mathcal{P}(N_X(b(o, r)) = 0) \tag{3.2}$$

Similarly, the *nearest neighbour distance distribution function* $G(r) : [0, \infty) \to [0, 1]$ gives the probability that the ball around an arbitrary point of the process x with radius r, $b(x, r)$, contains its nearest neighbouring point of the process X. Assuming that the process is stationary we can assume that x is the origin. The nearest neighbour function $G(r)$ is given by

$$G(r) = 1 - \mathcal{P}_o(N_X(b(o, r) \setminus \{o\}) = 0) \tag{3.3}$$

where $\mathcal{P}_o$ is a conditional probability given that there is an event in the origin.

A more interpretive summary function can be constructed from the nearest neighbour function $G(r)$ and empty space function $F(r)$. The so-called J function is given by

$$J(r) = \frac{1 - G(r)}{1 - F(r)}, \quad \text{when} \quad F(r) < 1$$

The values for the summary functions for the three main types of point patterns are interpreted as follows

(i) For CSR point patterns the following are true for $r \geq 0$

$$\begin{aligned} F(r) &= G(r) = 1 - e^{-\lambda \pi r^2} \\ J(r) &\equiv 1 \end{aligned} \tag{3.4}$$

(ii) For regular point patterns, we have that for $r \geq 0$

$$\begin{aligned} F(r) &> 1 - e^{-\lambda \pi r^2} > G(r) \\ J(r) &> 1 \end{aligned} \tag{3.5}$$

(iii) For clustered patterns, we have that for $r \geq 0$

$$\begin{aligned} G(r) &> 1 - e^{-\lambda \pi r^2} > F(r) \\ J(r) &< 1 \end{aligned} \tag{3.6}$$

It is important to note that the G, F, and J functions are appropriate for describing the spatial structure at small scales, since they consider the nearest events, but cannot provide any information about the structure at larger scales. Further, we should be careful when interpreting values of the J function as $J \equiv 1$ does not imply that X is the homogeneous Poisson process (Bedford and Van den Berg, 1997). Moreover, since $\lim_{r \to \infty} 1 - F(r) = 0$ the variance of the estimate $\hat{J}(r)$ increases with increasing r.

3.2.2 Second-order characteristics

Ripley's K function proposed by Ripley (1977) is a second order summary function that can characterise the structure of a point pattern at different scales. For stationary and isotropic point processes with intensity λ, Ripley's K function has a straightforward interpretation. In particular, $\lambda K(r)$ gives the expected number of further points of the process X within distance r from an arbitrary point of the process x. As X is stationary, we can assume that x is the origin o. In mathematical terms, Ripley's K function is defined as

$$\lambda K(r) = E_o[N_X(b(o, r) \setminus \{o\})] \tag{3.7}$$

where E_o is a conditional expectation given that there is an event in the origin. The values of Ripley's K function for point patterns in $\mathbb{R}^d$, can be interpreted as follows

(i) For CSR patterns, $K(r) = \mid b(o,r) \mid, \quad r \geq 0$

(ii) For regular patterns, $K(r) < \mid b(o,r) \mid, \quad r \geq 0$

(iii) For clustered patterns, $K(r) > \mid b(o,r) \mid, \quad r \geq 0$

where $b(o,r)$ is the d-dimensional ball centered at the origin o with radius r. A more interpretative version of the K function is the so called centred L function. The centered L function is given by

$$L(r) - r = \sqrt[d]{\frac{K(r)}{b_d}} - r, \quad r > 0. \tag{3.8}$$

where b_d is the volume of the d-dimensional unit ball. The theoretical value for the CSR case is $L(r) - r \equiv 0$, and hence we can determine if a pattern is clustered or regular by comparing the value of the summary function directly with zero.

3.2.3 Edge corrections

Naive estimators of the summary functions ignore neighbouring points that might have not been observed, i.e. points outside of W, which makes the estimators biased. In point process literature, this issue is referred to as edge effects. An illustration of this issue is displayed in Figure 3.2.

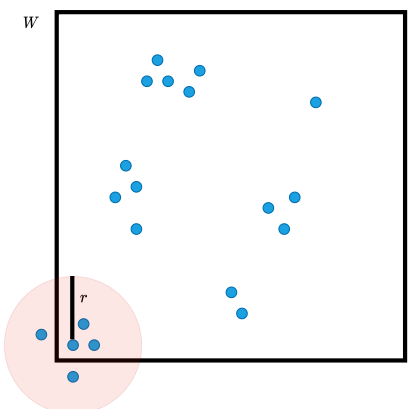

Figure 3.2: Example of edge effects. The points outside the observational window W are ignored in the estimation.

Therefore, to construct unbiased estimators, edge correction weights $C(x_i, x_j)$ are included within the estimators. Even though, the summary functions introduced earlier need to be edge corrected, this Section presents edge correction schemes only for the K function. The most common corrections for Ripley's K function are the *translation, isotropic* and *minus sampling* corrections. For a stationary point process the translation correction weights $C(x_i, x_j)$ are defined as follows.

$$C(x_i, x_j) = \frac{1}{\mid W \cap W_{x_i - x_j} \mid} \tag{3.9}$$

where $W_{x_i - x_j}$ denotes the translated window $W_{x_i - x_j}$ and $\mid \cdot \mid$ the Lebesgue measure. If the process is also isotropic, the isotropic correction is defined as

$$C(x_i, x_j) = \frac{\nu_1(\partial b(x_i, \mid\mid x_i - x_j \mid\mid) \cap W)}{2\pi \mid\mid x_i - x_j \mid\mid} \tag{3.10}$$

where ν_1 denotes the length of a curve, ∂ denotes the boundary of a set and $b(x_i, r)$ the ball centred at x_i with radius r. The above expression can be interpreted as the proportion of the perimeter of the ball that lies within the window W. In the minus sampling correction, only the points that have a distance larger than r from the boundary of the window ∂W are used as reference points - the ball centres - in the estimation of the summary function. A visual interpretation of the different edge corrections schemes is given in Figure 3.3

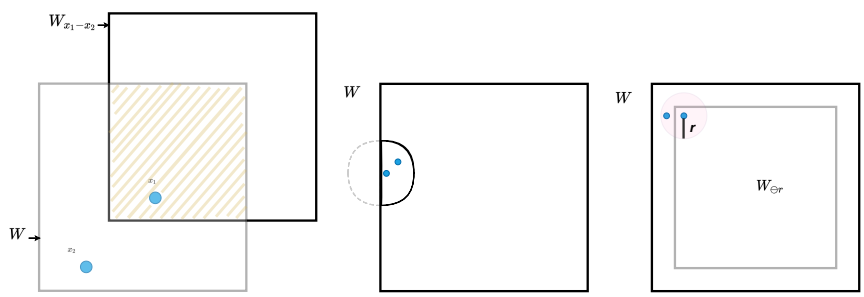

Figure 3.3: Illustration of the translation (left), isotropic (middle) and minus sampling (right) edge corrections

Therefore, an unbiased estimate for Ripley's K function is given by the following formula

$$\hat{K}(r) = \frac{1}{\hat{\lambda} n} \sum_{x_1, x_2 \in X \cap W}^{\neq} C(x_1, x_2) \mathbb{I}\{\mid\mid x_1 - x_2 \mid\mid \leq r\}, \quad r \geq 0, \tag{3.11}$$

where $C(x_i, x_j)$ is the edge correction weight, $\hat{\lambda}$ an estimate of the process intensity and n the total number of events.

3.2.4 Extensions of the K function

Bivariate K function

The K function can be extended for multi-type point processes. Let X_a and X_b be realizations of two stationary point processes observed in W, and let λ_a, λ_b be the intensities of X_a and X_b respectively. Then, $\lambda_b K_{a,b}(r)$ gives the expected number of further points of the process X_b in the d-dimensional ball with radius r centered at an arbitrary point x of the process X_a. If the process is stationary, x can be assumed to be the origin o. In mathematical notation this is expressed as follows

$$\lambda_b K_{a,b}(r) = E_o[N_{X_b}(b(o,r) \setminus \{o\})], \tag{3.12}$$

where E_o is a conditional expectation given there is an event of X_a in the origin o. Important to note that the *bivariate $K_{a,b}(r)$ function* coincides with the original Ripley's K function when $X_a = X_b$. An unbiased estimator for $K_{a,b}(r)$ can be obtained by

$$\hat{K}_{a,b}(r) = \frac{1}{\hat{\lambda}_b \hat{\lambda}_a \mid W \mid} \sum_{i=1}^{n_a} \sum_{j=1}^{n_b} C(x_{a_i}, x_{b_j}) \mathbb{I}\{0 < \mid\mid x_{a_i} - x_{b_j} \mid\mid \leq r\}, \quad r \geq 0, \tag{3.13}$$

where $C(x_{a_i}, x_{b_j})$ is an edge correction term, n_a and n_b are the numbers of points and $\hat{\lambda}_a$ and $\hat{\lambda}_b$ the intensity estimates of X_a and X_b, respectively.

Cylindrical K function

The isotropic K function is not an appropriate summary statistic for non-isotropic point patterns due to its symmetric structuring element, i.e. a d-dimensional ball. Directional K functions with non-symmetric structuring elements have been suggested as extensions of Ripley's K function for anisotropic point processes (see e.g Stoyan and Stoyan (1994); Rajala et al. (2018)). The three-dimensional end point clusters are anisotropic, as the behaviour in the xy plane differs from the behaviour in the z direction, i.e the end point clusters

have a cylindrical shape. The *cylindrical K function* $K^u_{cyl}(r)$ is a directional K function that uses a cylindrical structuring element (Møller et al., 2016). Similar to Ripley's K function the values of the cylindrical variant can be interpreted as the expected number of further events within distance r from an arbitrary event x, that is within a cylinder centred at x with a fixed half-width w and oriented towards u divided by the process intensity. Choosing appropriate directions u mainly depend on the nature of the application. For instance, the cylindrical $K^u_{cyl}(r)$ function is often estimated towards directions of the three main axes to test the assumption of isotropy. If the behaviour of $K^u_{cyl}(r)$ is significantly different in a direction u, then this indicates that the data are of anisotropic nature. An unbiased estimator for $K^u_{cyl}(r)$ is given by

$$K^u_{cyl}(r) = \frac{1}{\hat{\lambda^2}} \sum_{x_1,x_2 \in X \cap W}^{\neq} C(x_1, x_2)[x_1 - x_2 \in B^u(r, w)], \qquad r > 0, \tag{3.14}$$

where $C(x_1, x_2)$ is an edge correction term, $B^u(r, w)$ denotes the shape created by the intersection of a cylinder with fixed half-width w and direction u with spheres of radius $r > 0$ and $\hat{\lambda^2}$ is an estimate for the process squared intensity. As the half width w is fixed, $K^u_{cyl}(r)$ is defined as a function of distance r. Similarly to Ripley's K function, more interpretative variants can be defined for both the bivariate and cylindrical K functions. Hence, conclusions about the spatial structure of the point patterns are obtained by comparing the empirical curve with the line $y = 0$, corresponding to the CSR case. It is important to note that the spatial structure of a three dimensional pattern and the pattern consisting of the projected events to the plane might have different clustering behaviours. An example of such a case is illustrated in Figure 3.4. The pattern on the left (purple) is more clustered than the right pattern (red) in $\mathbb{R}^2$ but less clustered in $\mathbb{R}^3$. Further the differences in the structuring elements of the isotropic K function and the cylindrical K function oriented towards the z-axis are also illustrated.

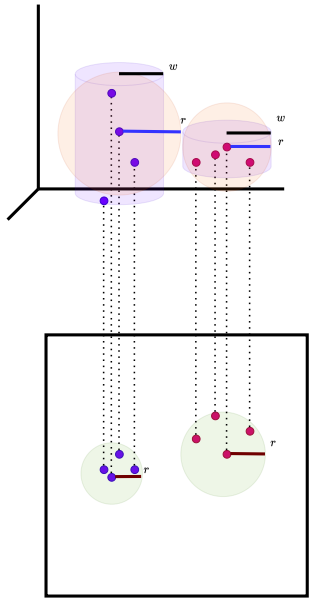

Figure 3.4: Illustration of potential differences in clustering in different dimensions. The projections of the "red" pattern are less clustered in $\mathbb{R}^2$ but more clustered than the "purple" pattern in $\mathbb{R}^3$. The structuring elements for the Ripley's K and cylindrical K functions are also illustrated.

Pooled K function

The aforementioned spatial summary functions are appropriate for describing the spatial structure of a single point pattern. When point pattern replicates are available, the summary functions can be extended to characterize the average spatial structure. For instance, the ENF data set is hierarchically structured into groups depending on the neuropathy severity, subjects within those groups, and several samples within each subject, and we want to compare the average spatial structure of the ENF patterns between the groups. The following methodology can be applied to extend the sample-wise summary functions to subject and group wise functions. Firstly, samplewise summary functions $K_{ij}(r)$ for sample $j \in \{1, ..., m_i\}$ of subject i can be estimated for each point pattern. Then, subject specific $\bar{K}_i(r)$ functions can be obtained as a weighted mean of the $K_{ij}(r)$ functions for all subjects $i \in \{1, ..., m\}$ as

$$\bar{K}_i(r) = \sum_{j=1}^{m_i} w_{ij} K_{ij}(r) \tag{3.15}$$

Finally, the subjectwise $\bar{K}_i(r)$ functions are weighted to obtain the groupwise $\bar{K}_g(r)$ function for the group g.

$$\bar{K}_g(r) = \sum_{i=1}^{m} w_i \bar{K}_i(r) \tag{3.16}$$

Several weight schemes can be applied to calculate the weights. As our samples cannot be assumed to have the same intensity, we used a square number weight scheme (Diggle et al., 2000). An explicit description of this weight scheme is as follows. Let n_{ij} be the number of points in sample j of subject i, and let $n_i = \sum_{j=1}^{m_i} n_{ij}$ be the total number of points in the samples from subject $i \in \{1, ..., m\}$. Then the square point number weights for the groupwise $\bar{K}_g(r)$ and subjectwise $\bar{K}_i(r)$ are given by

$$w_i = \frac{n_i^2}{\sum_{k=1}^{m} n_k^2}, \quad w_{ij} = \frac{n_{ij}^2}{\sum_{k=1}^{m_i} n_{ik}^2} \tag{3.17}$$

3.2.5 Mark correlation function

Often in applications numerical quantities, often referred as marks, are attached to the points. Generally, the marks are either integers, i.e different types of points in multi-type point patterns, or real valued numbers, i.e size related features such as height, diameter or width, even though functional marks are also possible. The mark correlation function is a second order characteristic for marked point processes able to detect spatial dependencies between the marks. The classical mark correlation function $K_{mm}(r)$ for quantitative marks is defined as follows.

$$K_{mm}(r) = \frac{c_{mm}(r)}{\mu^2} \quad r \geq 0 \tag{3.18}$$

where $c_{mm}(r) = E_{o,r}(m_o \cdot m_r)$ is the conditional expectation given that there is a point of the process in the origin and a point distance r away and $\mu^2 = c_{mm}(\infty)$ is the squared mean mark. The mark correlation function can be interpreted as follows

(i) If there is no correlation between the marks, then $K_{mm}(r) \equiv 1$.

(ii) If there is a negative correlation between the marks, for instance, there is competition between the points, we expect smaller than average marks for close points and hence $K_{mm}(r) < 1$.

(iii) If there is a positive correlation between the marks, for instance, the points benefit from being close together, we expect larger than average marks and hence $K_{mm}(r) > 1$.

Generalisations of the mark correlation function through the test function $t(m_o, m_r)$ can be defined in a natural way. The classical mark correlation function (Stoyan, 1984) is obtained with the test function $t(m_o, m_r) = m_o \cdot m_r$. An unbiased estimator of $K_{mm}(r)$ for $r \geq 0$ is given by

$$\hat{K}_{mm}(r) = \frac{1}{\hat{\lambda}^2 \hat{\mu}^2} \sum_{x_1, x_2 \in X \cap W}^{\neq} C(x_1, x_2) m(x_1) m(x_2) \mathbb{I}\{|| \, x_1 - x_2 \, || \leq r\}, \quad (3.19)$$

where $\hat{\lambda}$ is an estimate for the process intensity, $\hat{\mu}$ is an estimate for the mean of the mark distribution and $C(x_1, x_2)$ is an edge correction term.

Simulation envelopes under the null hypothesis that there is no correlation between the marks, can be constructed using a Monte Carlo method. In particular, at each iteration of the method the marks are randomly permuted between the points, keeping the locations of the points fixed, and the mark correlation function for the permuted marked configurations is computed. Simulations using this method construct marked point patterns with randomly labeled marks which are then used to create simulation based envelopes.

3.3 Point process models for clustered patterns

This Section focuses on point process models for clustered patterns. The Neyman-Scott family of cluster point process models is described first, followed by cluster models developed specifically for the ENFs.

3.3.1 Neyman-Scott point processes

Neyman-Scott point processes are cluster processes introduced by Neyman and Scott (1952) to model the locations of galaxies in space. The construction of a Neyman-Scott point process is rather simple. First, a Poisson point process P with intensity λ_p, often referred to as the parent process, is constructed. Then, a distribution for the number of daughter points N_c per cluster centre $c \in P$ is considered. The daughter points $x \in X_c$ are distributed in space according

to a scattering distribution δ. The final process X is then $X = \cup_c X_c$, hence the parent points are not observed.

A Neyman-Scott process X is stationary and if the scattering distribution is isotropic then X is also isotropic. Moreover, first and second order properties of X can be derived explicitly. Let $\alpha = E[N_c]$ be the expectation of the offspring distribution N_c, then the intensity of X is given by

$$\lambda = \lambda_p \alpha \tag{3.20}$$

Now let $p_k = \mathcal{P}(N_c = k)$, for $k \in \mathbb{N} \cup \{0\}$ and $F_d(r)$ be the distribution function of the random distance between two independent points in the same cluster X_c. Then, Ripley's K function for X is given by

$$K(r) = \pi r^2 + \frac{1}{\lambda \alpha} \sum_{i=2}^{\infty} p_i i(i-1) F_d(r), \quad r \geq 0 \tag{3.21}$$

The most notable examples of Neyman-Scott point processes are the Matérn and Thomas cluster point processes. In both point process models, the distribution of the random number of offspring follows a Poisson distribution with expectation α, that is $N_c \sim Poisson(\alpha)$. In the Matérn cluster process, the scattering distribution δ is a uniform distribution in the ball $b(c, R)$, for $c \in P$ and some radius parameter R. In the Thomas cluster process, δ is a Gaussian distribution with variance parameter σ. In both cases, δ is isotropic and hence X is a stationary and isotropic process. When the distribution of N_c is considered to be a discrete distribution other than Poisson, generalisations of the Matérn and Thomas processes can be obtained (see e.g Andersson and Mrkvička (2020)).

3.3.2 Cluster models for ENFs

This section, aims to give a brief review of the most relevant models found in the literature. We recall that the Neyman-Scott processes assume that the parent process is completely spatially random. If we further assume that the base point patterns represent the parent patterns for the end points, then Neyman-Scott are not appropriate models, since the base point patterns are clustered. As a result in previous studies on the nerve fibers, different type of cluster models for the planar spatial structure of the endpoints were suggested. The models presented here are models for the end points, and are constructed conditioned on the empirical base point patterns. Each model, consists of three main components, namely the length L, angle Φ, and tree size S, and

distributions for every component are suggested. The main assumption that is common in both models is the independence between the different components, which simplifies the parameter estimation procedure significantly.
The Non-Orphan Cluster (NOC) model (Olsbo et al., 2013) is given by

$$\begin{aligned} &L \sim Gamma(\alpha, \beta) \\ &\Phi \mid \mu \sim VonMises(\mu, \kappa) \\ &S \sim Jonquiere(\delta, \gamma) \end{aligned} \tag{3.22}$$

where μ is the so called open space direction, defined for each base point as the direction opposite to the closest other base point.

The Uniform Cluster Centre (UCC)(Andersson et al., 2016) is given by

$$\begin{aligned} &L \sim Gamma(\alpha, \beta) \\ &\Phi \mid \mu \sim VonMises(\mu, \kappa) \\ &S \sim NegativeBinomial(k, p) \end{aligned} \tag{3.23}$$

where there is no preference for μ.

4 General statistical tools

In this Section, some general tools used in the analysis of the ENFs point patterns are briefly desribed.

4.1 Metropolis-Hastings algorithm

Markov Chain Monte Carlo (MCMC) methods are statistical methods for inference and simulation from a target density $\pi(x)$ (see e.g Brooks et al. (2011)). If certain conditions are satisfied, a Markov chain $Y_0, Y_1, ...$ having the target distribution as its limiting distribution can be constructed. Metropolis-Hastings algorithm is an MCMC algorithm, that requires the target distribution to have probability density (or probability mass) function to be known up to a constant (Metropolis et al., 1953; Hastings, 1970). Hence, Metropolis-Hastings algorithms are also useful for simulating spatial point processes defined by an unnormalised density h. The algorithm described in this section conditions on the number of points in the point pattern, i.e $N_X(B) = n$. Therefore, we are interested in simulating from the conditional unnormalised density h_n such as

$$\pi(x_1, x_2, ..., x_n) \propto h_n(\{x_1, x_2, ..., x_n\}). \tag{4.1}$$

If certain conditions are satisfied, the algorithm creates a Markov chain of point configurations $Y_0, Y_1, ...$ whose stationary distribution converges to the target distribution of X. Let I_k denote the index of the point to be updated at iteration k of the algorithm. In a *systematic updating scheme* (Møller and Waagepetersen, 2004) we cycle through each point in every iteration as follows

$$I_0 = 1, ..., I_{n-1} = n, I_n = 1, ..., I_{2n-1} = n, ...$$

Given that the state at iteration k, $I_k = i$ and $Y_k = \bar{x} = (x_1, ..., x_n)$, we propose a new point $\xi \sim q_i(\bar{x}, \cdot)$ from a proposal density. The Hastings ratio $r_i(\bar{x}, \xi)$ is given by

$$r_i(\bar{x}, \xi) = \frac{h_n((\bar{x} \setminus x_i) \cup \xi) q_i((x_1, ..., x_{i-1}, \xi, x_{i+1}, ..., x_n), x_i)}{h_n(\bar{x}) q_i(\bar{x}, \xi)}. \tag{4.2}$$

Choosing a symmetric proposal, i.e. a proposal density such that $q_i(x, y) = q_i(y, x)$, simplifies the Hastings ratio $r_i(\bar{x}, \xi)$ to

$$r_i(\bar{x}, \xi) = \frac{h_n((\bar{x} \setminus x_i) \cup \xi)}{h_n(\bar{x})}. \tag{4.3}$$

Further, if we assume that the unconditional process is Markov, the expression for the Hastings ratio can be further simplified. A proposed state is then accepted with acceptance probability $a_i(\bar{x}, \xi)$ given by

$$a_i(\bar{x}, \xi) = \min(1, r_i(\bar{x}, \xi)) \tag{4.4}$$

Moreover, properties of the Markov chain created by the specific algorithm, such as irreducibility and reversibility can be proved. For a more mathematically rigorous treatment to the subject you are referred to Chapter 7 in Møller and Waagepetersen (2004). In Paper II, a Metropolis-Hastings algorithm with uniform proposal was used to simulate from the model. A pseudo-algorithm for a generic Metropolis-Hastings for point processes with conditional density h_n and fixed number of points is given in Algorithm 1.

Algorithm 1:

Result: A realisation from X given $N_X(B) = n$
Set $Y_0 = (x_1, ..., x_n)$;
for $m = 0, \ldots, M$ **do**
  Given that $Y_m = \bar{x}$;
  for $j = 1, \ldots, n$ **do**
    Draw $\xi \sim \mathrm{q}_j(\bar{x}, \cdot)$;
    Calculate $r_j(\bar{x}, \xi)$ using (4.2);
    Calculate $a_j(\bar{x}, \xi)$ using (4.4);
    Draw $U \sim \text{Uniform}(0, 1)$;
    if $U < a_j(\bar{x}, \xi)$ **then**
      Set $Y_m = (x_1, ..., x_{j-1}, \xi, x_{j+1}, ..., x_n)$
    else
      Set $Y_m = \bar{x}$
    end
  end
end

4.2 Shift plots and qq plots

The shift function introduced in Doksum and Sievers (1976) is a statistical tool for comparing two distributions, graphically. Let $X \sim F$ and $Y \sim G$, the shift function is defined as the function $\Delta(x)$ such as $F(x) = G(x + \Delta(x))$. Solving for $\Delta(x)$ we get that $\Delta(x) = G^{-1}(F(x)) - x$. Hence, $\Delta(\cdot)$ expresses the amount of 'shift' required so that X and Y coincide. Further, $\Delta(x) \equiv 0$ implies that X and Y have the same distribution. The qq (quantile quantile) plot is closely related to the shift function. When comparing two random samples with a qq-plot, the quantiles of one sample are plotted against the quantiles of the other. If they have the same distribution, the points should fall on the line $y = x$. The shift function $\Delta(x)$ is the shortest distance between the qq-plot points and the line $y = x$.

Simultaneous 95% confidence bands for $\Delta(x)$ can be created using the Kolmogorov-Smirnov statistic. Hence, if the line $y = 0$ lies within the confidence bands of the estimated shift function $\hat{\Delta}(x)$ then F and G are statistically indistinguishable. One advantage of this statistical tool is that if F and G differ, visual inspection of the shift plot can provide information on how the distributions differ. Example on how shift plots can be used to compare the distribution of two random random variables are shown in Figure 4.1.

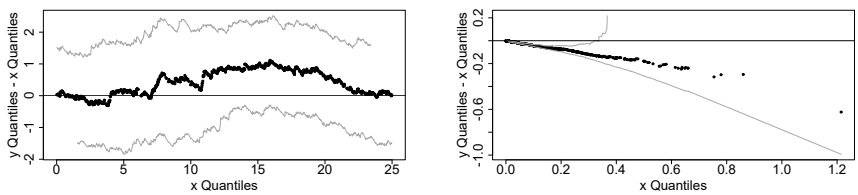

Figure 4.1: Illustration of the shift plots for two random variables that are statistically indistinguishable (left) and from different distributions (right), with 95% confidence bands based on the Kolmogorov-Smirvov statistic.

5 Summary of papers

5.1 Paper I

In this paper, we studied the 3D spatial structure of epidermal nerve fibers by representing each nerve tree by the base point, first branching point and end points. For the analysis, we considered skin samples obtained from the feet of 32 healthy volunteers and 8 mild diabetic subjects. We included the first-branching point patterns into the analysis, since they are a naturally better choice for endpoint cluster centers than the base points, and unlike the base points, that are clustered, they are indistinguishable from completely spatially random patterns. Moreover, we compared the three-dimensional structure of the endpoint patterns between the two disease groups using summary functions for point patterns. Even though, the planar point patterns of the mild group are more clustered than the point patterns in the healthy group, no significant difference in clustering was found between the three-dimensional point patterns of the two groups in terms of second-order summary statistics.

To study the tree structure within the individual nerve trees, we considered the branch lengths and angles of the first segments, the tree segment connecting the base to the branching points, and the later segments, the tree segments connecting the branching points to the end points. We used shift plots to compare the branch lengths and angular distributions of the two tree segments. Our statistical analysis suggested that the first segment length is significantly larger and the first segments grow more vertically than the later segments. Further, we compared the tree structure between the groups. Our results indicated that there are significant differences between the angular distributions of the later segments of the two groups.

Moreover, we extended the concept of reactive territories, in our paper called epidermal active territories (EAT), introduced in Andersson et al. (2016) for 2D point patterns, to 3D point patterns. The epidermal active territory is

defined as the volume of the area in the epidermis covered by individual nerve fibers. Our results showed that the total volume of the epidermis covered by the nerve trees was larger in the healthy group than in the mild group. In addition, possible competitive behavior between individual nerves was examined by using the mark correlation function of the base point process with the epidermal active territories as marks. No spatial dependencies were detected between the marks.

Finally, we proposed a two-step point process model for the end points conditioned on the base point patterns. In the first step, the first branching points are sent towards open space, as in the NOC model in Olsbo et al. (2013). In the second step, the endpoint clusters are constructed around the simulated branching points. The two-dimensional version of the model fitted the data quite well, while the three-dimensional version revealed that there are interactions between the endpoints that were not captured by the model.

5.2 Paper II

Inspired by Christoffersen et al. (2021) we developed a 3D point process model, that allowed the end points to interact with each other. The model consisted of two steps. In the first step, the planar point patterns were obtained using the two-dimensional version of the model introduced in Paper I. In the second step, the process in the z-direction X_z given the planar process X_p was constructed using a pairwise interaction Markov random field model. In the model, two points are considered neighbors if they lie within a cylindrical interaction region centered in one of the points. The conditional density consisted of two parts, one modelling the cylindrical attraction between the endpoints and a hardcore ball not allowing points to be closer than the points in the data. The parameters of the model, $\theta = (h, w, t, \gamma)$, were estimated by maximizing the pseudolikelihood over a grid of values for the cylinder parameters (w, t) using the minimum distance between the endpoints in the data multiplied by $\frac{n-1}{n}$ as an estimate for the hardcore distance h. To reduce the bias due to edge effects, minus sampling was used. The parameter estimates suggest that in both groups, after a hardcore radius h the end points attract each other. The attraction is larger in the healthy group than in the mild diabetic group.

Furthermore, a Markov chain Monte Carlo algorithm, where the number of points in the planar process X_p are fixed, was used to simulate from the model. We used a systematic updating scheme cycling over the point indexes 1 to n and using a uniform proposal for a new point in W_z. Due to the anisotropic nature of the data the goodness-of-fit of the model was evaluated using the

cylindrical K function. Simulations from the model were able to capture both the complete spatial structure of the endpoints and the structure of the endpoints with respect to their branching points. However, as the model utilises a Metropolis-Hastings algorithm, it is computationally expensive to simulate. Therefore, our goodness-of-fit analysis was limited to two arbitrary chosen healthy and two mild diabetic subjects. Finally, we would like to point out that the proposed methodology is generic, and hence can be used for point pattern data in general.

6 Conclusion and future work

To the best of our knowledge, this is the first study that analyzed the nerve fiber patterns in three dimensions. In contrast to the planar patterns, second order analysis of the patterns indicated that there is no significant difference in clustering between the data from the two disease groups. As a result, the clusters in the diabetic samples are tighter in the xy direction, but there is no difference in the structure of the clusters in the three dimensions. Moreover, second order analysis of the first branching points patterns suggests that they are less clustered than the base points, indicating some repulsion between different endpoint clusters. In Paper I, we investigated the distributional properties of the nerve tree segments as well as competition between the nerve trees. Further, we developed a three dimensional point process model for the nerve tree structure. The two dimensional version of the model had a good fit, but the three-dimensional version failed to capture the ENF structure, indicating potential interactive behaviour between the ENFs. For this purpose in Paper II, a model allowing end points to interact in a cylindrical region was developed. Even though the methods and models have been developed having the ENF data in mind, they can be used for point pattern data in general.

As the primary goal of this thesis is to improve our understanding of the underlying biological mechanism that causes physiological changes in the structure of nerve fibers as a result of neuropathy, there are several potential future research topics to investigate. Diabetic nerve fiber patterns, for instance, can be considered as spatial thinnings of healthy nerve fiber patterns. Preliminary analysis on this topic revealed that independent random thinning is insufficient to describe this biological process, and hence more sophisticated thinning strategies must be investigated. However, thinning operations alone may not be sufficient, thus more complex models that allow for point addition and movement might have to be considered.

Bibliography

Andersson, C., Guttorp, P., and Särkkä, A. (2016). Discovering early diabetic neuropathy from epidermal nerve fiber patterns. *Statistics in medicine*, 35(24):4427–4442.

Andersson, C. and Mrkvička, T. (2020). Inference for cluster point processes with over-or under-dispersed cluster sizes. *Statistics and Computing*, 30(6):1573–1590.

Andersson, C., Rajala, T., and Särkkä, A. (2019). A bayesian hierarchical point process model for epidermal nerve fiber patterns. *Mathematical biosciences*, 313:48–60.

Bedford, T. and Van den Berg, J. (1997). A remark on the van lieshout and baddeley j-function for point processes. *Advances in Applied Probability*, 29(1):19–25.

Brooks, S., Gelman, A., Jones, G., and Meng, X.-L. (2011). *Handbook of markov chain monte carlo*. CRC press.

Chiu, S. N., Stoyan, D., Kendall, W. S., and Mecke, J. (2013). *Stochastic geometry and its applications*. John Wiley & Sons.

Christoffersen, A. D., Møller, J., and Christensen, H. S. (2021). Modelling columnarity of pyramidal cells in the human cerebral cortex. *Australian & New Zealand Journal of Statistics*.

Diggle, P. J., Mateu, J., and Clough, H. E. (2000). A comparison between parametric and non-parametric approaches to the analysis of replicated spatial point patterns. *Advances in Applied Probability*, 32(2):331–343.

Doksum, K. A. and Sievers, G. L. (1976). Plotting with confidence: Graphical comparisons of two populations. *Biometrika*, 63(3):421–434.

Garcia, N. L., Guttorp, P., and Ludwig, G. (2020). Interacting cluster point process model for epidermal nerve fibers. *Spatial Statistics*, 35:100414.

Ghorbanpour, F., Särkkä, A., and Pourtaheri, R. (2021). Marked point process analysis of epidermal nerve fibres. *Journal of Microscopy*.

Hastings, W. K. (1970). Monte carlo sampling methods using markov chains and their applications.

Illian, J., Penttinen, A., Stoyan, H., and Stoyan, D. (2008). *Statistical Analysis and Modelling of Spatial Point Patterns*. John Wiley & Sons.

Kennedy, W. R., Nolano, M., Wendelschafer-Crabb, G., Johnson, T. L., and Tamura, E. (1999). A skin blister method to study epidermal nerves in peripheral nerve disease. *Muscle & Nerve: Official Journal of the American Association of Electrodiagnostic Medicine*, 22(3):360–371.

Kennedy, W. R. and Wendelschafer-Crabb, G. (1993). The innervation of human epidermis. *Journal of the neurological sciences*, 115(2):184–190.

Kennedy, W. R., Wendelschafer-Crabb, G., and Johnson, T. (1996). Quantitation of epidermal nerves in diabetic neuropathy. *Neurology*, 47(4):1042–1048.

Lauria, G., Bakkers, M., Schmitz, C., Lombardi, R., Penza, P., Devigili, G., Smith, A. G., Hsieh, S.-T., Mellgren, S. I., Umapathi, T., et al. (2010). Intraepidermal nerve fiber density at the distal leg: a worldwide normative reference study. *Journal of the Peripheral Nervous System*, 15(3):202–207.

Metropolis, N., Rosenbluth, A. W., Rosenbluth, M. N., Teller, A. H., and Teller, E. (1953). Equation of state calculations by fast computing machines. *The journal of chemical physics*, 21(6):1087–1092.

Møller, J., Safavimanesh, F., and Rasmussen, J. G. (2016). The cylindrical-function and poisson line cluster point processes. *Biometrika*, 103(4):937–954.

Møller, J. and Waagepetersen, R. (2004). *Statistical Inference and Simulation for Spatial Point Processes*. Boca Raton: CRC Press.

Myllymäki, M., Panoutsopoulou, I., and Särkkä, A. (2012). Analysis of spatial structure of epidermal nerve entry point patterns based on replicated data. *Journal of microscopy*, 247(3):228–239.

Neyman, J. and Scott, E. (1952). A theory of the spatial distribution of galaxies. *The Astrophysical Journal*, 116:144.

Olsbo, V., Myllymäki, M., Waller, L. A., and Särkkä, A. (2013). Development and evaluation of spatial point process models for epidermal nerve fibers. *Mathematical biosciences*, 243(2):178–189.

Rajala, T., Redenbach, C., Särkkä, A., and Sormani, M. (2018). A review on anisotropy analysis of spatial point patterns. *Spatial Statistics*, 28:141–168.

Ripley, B. D. (1977). Modelling spatial patterns. *Journal of the Royal Statistical Society: Series B (Methodological)*, 39(2):172–192.

Stoyan, D. (1984). On correlations of marked point processes. *Mathematische Nachrichten*, 116(1):197–207.

Stoyan, D. and Stoyan, H. (1994). *Fractals, random shapes and point fields: methods of geometrical statistics*, volume 302. Wiley-Blackwell.

Waller, L. A., Särkkä, A., Olsbo, V., Myllymäki, M., Panoutsopoulou, I. G., Kennedy, W. R., and Wendelschafer-Crabb, G. (2011). Second-order spatial analysis of epidermal nerve fibers. *Statistics in Medicine*, 30(23):2827–2841.